Critical reflectance derived from MODIS: Application for the retrieval of aerosol absorption over desert regions

Kelley C. Wells,[1,2] J. Vanderlei Martins,[3] Lorraine A. Remer,[4] Sonia M. Kreidenweis,[1] and Graeme L. Stephens[1,5]

Received 17 September 2011; revised 21 November 2011; accepted 23 November 2011; published 1 February 2012.

[1] The determination of aerosol direct radiative forcing over desert regions requires accurate information about the aerosol single-scattering albedo (SSA); however, the brightness of desert surfaces in the visible and near-IR range complicates the retrieval of aerosol optical properties using passive space-based measurements. Here we use the critical reflectance method to retrieve spectral aerosol absorption from space over North Africa, a desert region that is predominantly impacted by absorbing dust and biomass burning aerosol. We examine the sensitivity of the critical reflectance parameter to aerosol physical and optical properties that are representative of the region, and we find that the critical reflectance has low sensitivity to assumptions of aerosol size and refractive index for dust-like particles, except at scattering angles near 180°, which should be avoided with this method. We use our findings to retrieve spectral SSA from critical reflectance derived from Moderate Resolution Imaging Spectroradiometer (MODIS) reflectances in the vicinity of two Aerosol Robotic Network (AERONET) stations: Tamanrasset, in the Algerian Sahara, and Banizoumbou, in the Sahel. We retrieve lower aerosol SSAs at Banizoumbou, which is often impacted by dust-smoke mixtures, and higher SSAs at Tamanrasset, where pure desert dust is the dominant aerosol. Our results generally fall within the AERONET uncertainty envelopes, although at Banizoumbou we retrieve a spectral dependence different from that of AERONET. On the basis of our analysis, we expect to be able to retrieve SSA from critical reflectance for pure dust with an uncertainty of 0.02 and to provide spatial and spectral SSA information that will help reduce current uncertainties in the aerosol radiative forcing over desert regions.

Citation: Wells, K. C., J. V. Martins, L. A. Remer, S. M. Kreidenweis, and G. L. Stephens (2012), Critical reflectance derived from MODIS: Application for the retrieval of aerosol absorption over desert regions, *J. Geophys. Res.*, *117*, D03202, doi:10.1029/2011JD016891.

1. Introduction

[2] Estimating the direct radiative effect of aerosols from space is an essential component in constraining climate prediction models and narrowing uncertainties in determining the magnitude of climate change. The wealth of global data sets currently available from ground and space-borne sensors provides the possibility of quantifying the perturbation of both solar and terrestrial radiation due to particulate matter of both anthropogenic and natural origin. Although there have been significant advances in retrieving the physical properties of atmospheric aerosol from satellite-based instruments [e.g., *Remer et al.*, 2005; *Kahn et al.*, 2010] the effects of certain aerosol types over some regions of the globe still remain highly uncertain. Specifically, the direct effect over land is not well known [*Yu et al.*, 2006], especially over bright land surfaces where it is difficult to separate the effects of surface and aerosol contributions in the visible and near IR [*Kaufman et al.*, 1997]. Additionally, the direct effect over land depends strongly on the absorption properties of the aerosol and the spectral albedo of the underlying surface. Over dark surfaces, aerosols scatter more radiation back to space than does the underlying surface, brightening the scene from space and cooling the Earth-atmosphere system. The same aerosol over brighter surfaces may absorb some of the scattered radiation from the underlying surface, acting to darken the scene from space and exerting a warming effect [*Kaufman*, 1987]. The change from brightening to darkening,

[1]Department of Atmospheric Science, Colorado State University, Fort Collins, Colorado, USA.
[2]Now at Department of Soil, Water and Climate, University of Minnesota, Twin Cities, Saint Paul, Minnesota, USA.
[3]Department of Physics and Joint Center for Earth Systems Technology, University of Maryland, Baltimore County, Baltimore, Maryland, USA.
[4]NASA Goddard Space Flight Center, Greenbelt, Maryland, USA.
[5]Now at Jet Propulsion Laboratory, Pasadena, California, USA.

0148-0227/12/2011JD016891

cooling to warming, is dependent mainly on the surface reflectance and the absorption properties of the aerosol.

[3] The aerosol single-scattering albedo (SSA), which is the ratio of the aerosol scattering to extinction (absorption + scattering) coefficients, is the parameter commonly used to quantify the effect of aerosol absorption, and it will drive the sign of the top-of-atmosphere (TOA) forcing for a given surface albedo. The value at which this transition point occurs has been referred to as the critical single-scattering albedo [*Liao and Seinfeld*, 1998]; over desert, this value can be high. As a result, the top-of-atmosphere forcing over bright desert surfaces is very sensitive to small changes in absorption. A modeling study by *Solmon et al.* [2008] showed that a variation in the 0.55 μm SSA from 0.9 to 1.0 (for submicron aerosol) can change the sign of the TOA forcing over the entire Saharan desert, altering atmospheric heating rates and modifying precipitation patterns associated with the West African monsoon. Additionally, knowledge of the aerosol SSA impacts the accurate retrieval of aerosol optical depth over bright land surfaces. *De Almeida Castanho et al.* [2008] found that a SSA uncertainty of 0.1 could lead to an uncertainty in optical depth greater than 100% over surfaces with high reflectance.

[4] Thus, more accurate knowledge of aerosol absorption properties is critical for understanding the impact of aerosols on climate in desert regions, both for determining their overall radiative effect, and for tracking their size, total amount, and transport patterns. There have been many efforts in recent years to quantify aerosol absorption using space-based measurements. The first measurements were qualitative retrievals in the ultraviolet (UV) spectral range from the Total Ozone Mapping Spectrometer (TOMS) [*Hsu et al.*, 1996; *Herman et al.*, 1997]. Currently, space-based retrievals of aerosol SSA are available in the UV from the Ozone Monitoring Instrument (OMI) [*Torres et al.*, 2007], and in the visible spectral range from the Multiangle Imaging Spectroradiometer (MISR) [*Kalashnikova and Kahn*, 2006] and the Moderate Resolution Imaging Spectroradiometer (MODIS) Deep Blue product [*Hsu et al.*, 2004, 2006]. Additional studies combining multiple satellite sensors in the NASA A-train have been implemented [e.g., *Jeong and Hsu*, 2008; *Satheesh et al.*, 2009], but these also only provide aerosol information in the UV. The critical reflectance [*Fraser and Kaufman*, 1985] is another method that can be used to derive SSA from existing satellite data, with the benefit that it can be applied over the full visible and near-IR spectral range currently used in operational aerosol retrievals.

[5] The application of the critical reflectance principle to derive aerosol absorption from satellite measurements was first demonstrated by *Fraser and Kaufman* [1985] and *Kaufman* [1987] using Landsat data. It has subsequently been applied to biomass burning regimes using MODIS data [*Zhu et al.*, 2011] and to Saharan dust using Landsat [*Kaufman et al.*, 2001] and MODIS data [*Yoshida and Murakami*, 2008]. It harnesses the principle that, for a given aerosol of fixed SSA and phase function, there is a certain surface reflectance at which the reflectance at TOA is nearly insensitive to aerosol loading. This "critical reflectance" occurs when the enhanced aerosol backscattering at TOA is balanced by the enhanced absorption of the upwelling radiation by the aerosol layer. One can derive the critical reflectance by comparing two satellite images with pixels of variable surface reflectance, identical geometries and the same aerosol type, but different aerosol loadings. Taking advantage of the variability in surface reflectance, the critical reflectance will be the satellite-measured reflectance that is the same in the two images for the same surface location viewed by the same geometry. At the critical reflectance, additional aerosol loading does not change the TOA reflectance value because enhanced backscatter is balanced by enhanced absorption. The method requires the following assumptions: (1) the aerosol optical depth for each image is constant over the area in which the comparison between the two images occurs, (2) there is enough surface variability within the selected image, but the surface reflectance for each pixel is invariant between the two days, and (3) the background aerosol phase function, SSA, and gas columns are similar between the two days.

[6] *Kaufman* [1987] outlined some of the limitations and sources of uncertainty in applying the critical reflectance to estimate SSA, as did *Zhu et al.* [2011] in their assessment and application of the method over the Amazon rain forest and African savanna, but a full assessment of the utility of critical reflectance for retrievals over desert has not been reported to date. In this paper we outline our method of retrieving the critical reflectance from satellite data, using MODIS Level 1B data in the desert region of North Africa. We investigate the sensitivity of the critical reflectance parameter to assumed aerosol physical and optical properties at solar and viewing geometries that are representative of satellite-based observations, using the SBDART radiative transfer model and a T-matrix code. We use our findings to build look-up tables (LUTs) for retrieving spectral SSA from the MODIS-derived critical reflectance. Case study examples in the vicinity of two sites that are a part of the Aerosol Robotic Network (AERONET) [*Holben et al.*, 1998] in North Africa are shown, and evaluated with respect to the AERONET retrievals.

2. Method

2.1. Observations

[7] We derive the critical reflectance using Level 1B reflectances from the MODIS instrument onboard the NASA EOS Terra and Aqua satellites. Because the critical reflectance must be derived by comparing images with the same solar and viewing geometry, we obtain data for pairs of images with different aerosol loading that are 16 days apart as MODIS has a 16 day repeat orbit. We use reflectance data from the same seven bands (Bands 1–7, which span the spectral range from 0.47 to 2.13 μm) used in the operational MODIS aerosol algorithm, along with Band 26 (1.38 μm) for cloud screening purposes. At nadir, Bands 1 and 2 have a horizontal resolution of 0.25 km, Bands 3–7 have a horizontal resolution of 0.5 km, and Band 26 has a resolution of 1 km.

[8] To isolate the component of the reflectance that is due to aerosol scattering, we correct the reflectance data for absorption due to water vapor, ozone, and carbon dioxide, and screen for the presence of clouds within the image. The gaseous absorption correction is the same as that used in the operational MODIS aerosol retrieval algorithm [*Remer et al.*, 2006] and requires ancillary data on trace gas concentrations. Column precipitable water data from 1° × 1°

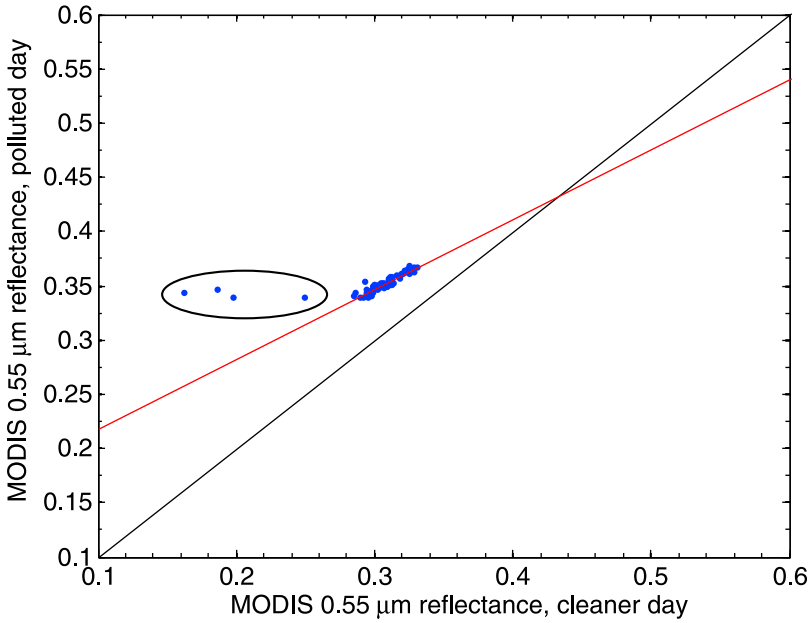

Figure 1. Scatterplot of polluted versus cleaner MODIS reflectances at 0.55 μm for one 10 $\times$ 10 pixel box. The black line is the one-to-one line; the red line is the linear fit determined using robust regression. The outliers circled in the plot were automatically eliminated by the robust fitting routine.

NCEP reanalysis (obtained from http://www.esrl.noaa.gov/psd/data/reanalysis/reanalysis.shtml) are used for the water vapor correction; the ozone correction is done using the 1° $\times$ 1° TOAST (Total Ozone Analysis using SBUV/2 and TOVS) column ozone product (obtained from http://www.osdpd.noaa.gov/ml/air/toast.html). We assume fixed global average values of optical depth for the carbon dioxide correction.

[9] We perform cloud screening on the reflectance data using the same technique as described by *Martins et al.* [2002] for the MODIS over-ocean cloud screening algorithm, which we have modified to be applicable over land. It consists of a combined test using the spatial homogeneity of the reflectance along with absolute reflectance thresholds. We use Band 3 (0.47 μm) to identify low clouds, and Band 26 (1.38 μm) to identify high clouds. Our algorithm constructs a 3 $\times$ 3 pixel mask that is flagged as cloud if the standard deviation of the reflectance of the 3 $\times$ 3 pixels is greater than 0.01 at 0.47 μm or 0.007 at 1.38 μm. It is also flagged as cloud if the gas-corrected reflectance in either of these bands exceeds a maximum threshold value (0.4 at 0.47 μm and 0.1 at 1.38 μm).

[10] To facilitate pixel-to-pixel comparison of two images, we remap the reflectance data onto an equal latitude-longitude grid. Small orbital shifts cause slight changes in the viewing and solar zenith angle for a given pixel relative to 16 days prior (typically less than two degrees); additionally, pixels become larger as the scanner moves away from nadir view. We aggregate the reflectances up to a resolution of 1.5 km.

[11] Once the data are remapped to the same grid, the area of a larger box upon which to retrieve a constant SSA is defined. The area must be large enough to contain some variability in surface reflectance, so that there is some dynamic range of reflectances on the cleaner day over which to perform a data regression. But, the box must not be too large as to avoid significant spatial variations in aerosol loading. For the retrievals presented here we choose an area of 10 $\times$ 10 pixels (15 $\times$ 15 km). Within each retrieval box the remapped reflectance data are matched in space, and the reflectances on the polluted day are regressed against the reflectances of the cleaner day. The slope and intercept are determined using a robust linear fitting procedure [*DuMouchel and O'Brien*, 1989], in order to give less weight to data outliers. An example scatterplot between polluted and cleaner reflectances at 0.55 μm from MODIS is shown in Figure 1. The point at which the fit line crosses the one-to-one line is the critical reflectance at TOA. The y intercept is related to the optical depth difference between the cleaner and the polluted day. If there are any missing data within the retrieval box due to cloud screening, no retrieval is performed within the box.

[12] Because the uncertainty in the measured reflectances from MODIS is only on the order of $\pm$2% [*Remer et al.*, 2005], too small to affect our retrieval, we assume that the uncertainty in the observed critical reflectance is a combination of the uncertainties associated with the data fitting routine and the assumptions listed in the introduction. We consider one measurement of the uncertainty due to data fitting to be the standard deviation of the residuals of the fit line:

$$\sigma_{resid} = \sqrt{\frac{\sum_{i=1}^{N} \left(y_i - y_{fit,i}\right)^2}{N-1}}, \quad (1)$$

where y_i is the TOA reflectance value of a single pixel on the polluted day and $y_{fit,i}$ is the y value of the linear fit to the TOA reflectance data. In order to consider the number of outliers in the determination of which pixels to keep from the retrieval, we also throw out a box if it contains more than 10 pixels with a residual reflectance greater than $2\sigma_{resid.}$

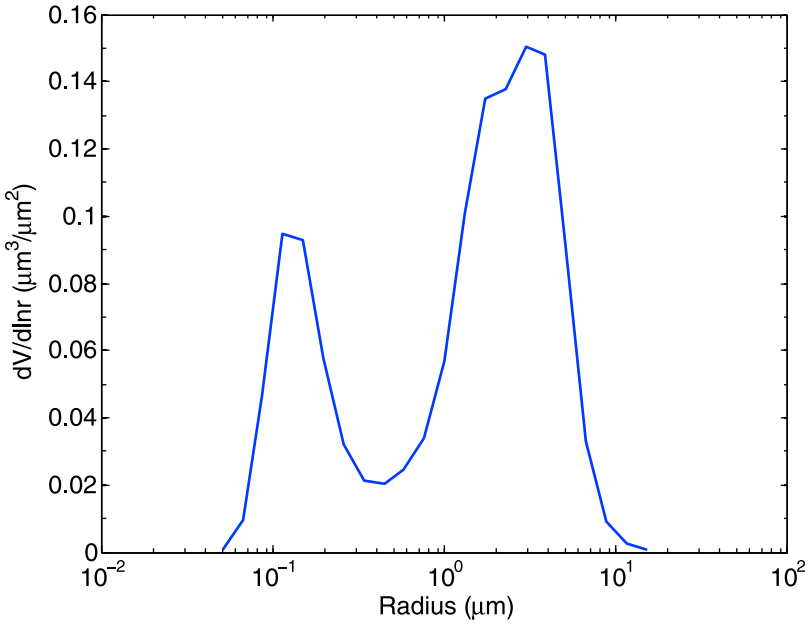

Figure 2. Bimodal aerosol size distribution taken from an AERONET almucantar retrieval at Banizoumbou on 19 January 2006.

2.2. Forward Model

[13] We use a standard, publicly available radiative transfer model, SBDART, to build a look-up table (LUT) of critical reflectance as a function of SSA for different assumed aerosol size distributions and refractive indices, as well as a range of solar and viewing geometries that are applicable to the MODIS instrument orbit and scanning characteristics. This section details the radiative transfer model setup, aerosol model assumptions and phase function calculations, and the LUT-building procedure.

[14] The Santa Barbara DISORT Atmospheric Radiative Transfer (SBDART) model [*Ricchiazzi et al.*, 1998] is a multistream radiative transfer model that uses the Discrete Ordinate Radiative Transfer code [*Stamnes et al.*, 1988] to integrate the radiative transfer equation for a plane-parallel vertically inhomogeneous atmosphere. We use version 2.4. The model can handle a maximum of 40 streams, but we use the default 20 streams for computational efficiency.

[15] The model setup we use ascribes 32 layers to the atmosphere: 25 equidistant layers between 0 and 25 km, 5 equidistant layers between 25 and 50 km, and 2 equidistant layers between 50 and 100 km. Gas column amounts and vertical profiles are assumed on the basis of the standard subarctic summer atmosphere contained in the SBDART database. Because we correct the MODIS data for gaseous absorption, we set column ozone, water vapor, and carbon dioxide concentrations to zero in the model. We apportion the total aerosol optical depth (AOD) as an exponential decay through the lowest 5 km of the atmosphere. This height was chosen on the basis of the average vertical profiles of aerosol extinction measured in the Sahel region during the Dust and Biomass Burning Experiment (DABEX) campaign [*Johnson et al.*, 2008]. Aerosol SSA and scattering phase function are assumed constant with height. Below the atmosphere, isotropic scattering from the surface is assumed.

[16] Aerosol phase functions and SSAs are modeled using a modified T-matrix code [*Dubovik et al.*, 2002] for the seven MODIS channels we use in the retrieval. The code simulates a population of particles as spheres, spheroids, or a mixture of both. The user specifies the particle size distribution, and the fraction of the total particle volume made up of spherical particles. We use 22 size bins evenly spaced on a log scale, ranging from 0.05 to 15 μm in radius, which is consistent with the length and range of the size distribution vector output by the standard AERONET retrieval [*Dubovik and King*, 2000]. We assume four different aerosol models: fine mode spheres, a coarse mode made of primarily spheroids (percent sphericity = 0.5%), bimodal spheres, and bimodal spheroids (percent sphericity = 4%). The bimodal size distribution (Figure 2) was taken from an AERONET retrieval over the Banizoumbou station on 19 January 2006, a date on which a dust and smoke mixture was intercepted near the site as part of the DABEX campaign [*Johnson et al.*, 2009]. For the coarse model, we simply assume the coarse mode of this distribution, and the fine mode for the fine model. The value chosen for percent sphericity of the bimodal spheroid distribution is assumed on the basis of the reported value from AERONET on 19 January 2006.

[17] For each wavelength and size model we assume the real refractive index, n_r, to be 1.53, which is the same value assumed in the MODIS operational algorithm from 0.47 to 0.86 μm for the dust-like aerosol model [*Remer et al.*, 2005]. We vary the imaginary part of the refractive index, n_i, from 0.0005 to 0.03 in order to simulate a wide range of aerosol absorption values. For each refractive index and wavelength, the code estimates the scattering phase function at 83 scattering angles, as well as the SSA of the particle population.

[18] The computed phase functions and SSAs for each size model and refractive index are input into SBDART to simulate TOA reflectances, as functions of assumed aerosol

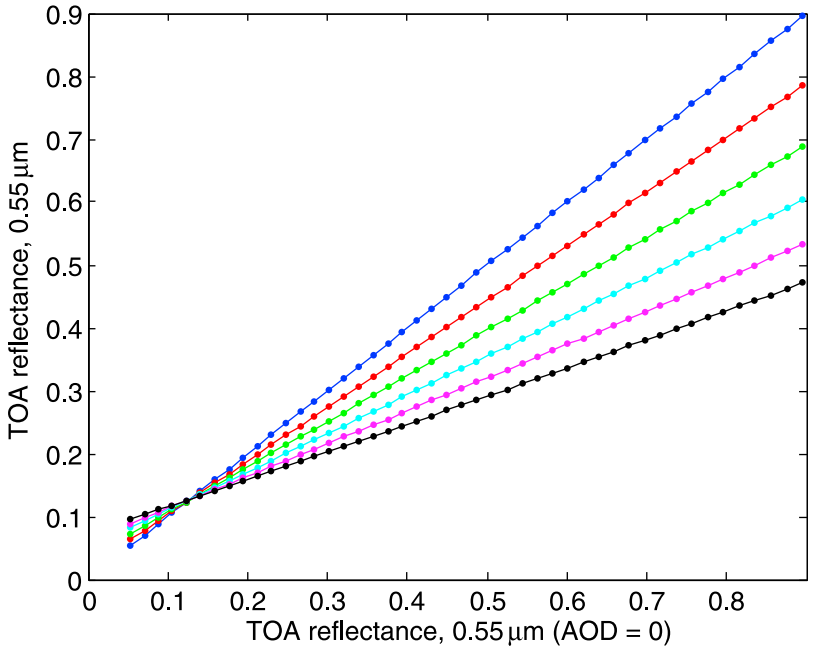

Figure 3. TOA reflectance for AOD = 0 (blue), 0.2 (red), 0.4 (green), 0.6 (cyan), 0.8 (magenta), and 1.0 (black) plotted against TOA reflectances for AOD = 0 for the coarse model at 0.55 μm, n_i = 0.01, solar zenith angle (SZA) = 24°, view angle = 60°, and relative azimuth = 120°.

optical depth and surface albedo, from which the critical reflectance values can be determined. We perform our simulations at the same geometries as the MODIS operational algorithm: nine solar zenith angles (6, 12, 24, 36, 48, 54, 60, 66, and 72°), 13 satellite view angles (0 to 72°, in increments of 6°), and 16 relative azimuths (0 to 180°, in increments of 12°). The AOD is varied from 0 to 1 in increments of 0.2, and the surface albedo is varied from 0 to 0.9 in increments of 0.02. For each solar/viewing geometry, aerosol size model, and SSA simulated, we compare the TOA reflectance for each simulated AOD to the TOA reflectance for AOD = 0 (Figure 3). The polluted-day TOA reflectance that corresponds to the intersection of the TOA reflectance curves with the one-to-one line is defined as the simulated critical reflectance. Because the critical reflectance is not completely insensitive to AOD, this intersection does not occur at a precise point, so we define the simulated critical reflectance as the average of the intersections of the TOA reflectance for AOD = 0.2, 0.4, 0.6, and 1.0 with the one-to-one line. We define the uncertainty in the simulated critical reflectance due to AOD variation as the standard deviation of the intersections of these curves.

[19] Example results of the simulated critical reflectance (R_{crit}) as a function of SSA for the fine and coarse aerosol models at 0.55 μm are shown in Figure 4a for SZA = 24°, view angle = 60° and relative azimuth = 120°. Note that increasing R_{crit} corresponds to increasing SSA, although the relationship is not linear. The less absorbing the aerosol, the more it will reflect radiation back to space and the higher the R_{crit} value will be. As such, the critical reflectance is more sensitive to SSA as absorption decreases. Although R_{crit} is the simulated parameter, we use relationships similar to the illustration in Figure 4a to derive SSA from R_{crit} measured from MODIS. The process is illustrated using the arrows that lead from an R_{crit} value on the y axis to a point on the curve and then down to intersect a SSA value on the x axis. Error estimation using this process is outlined in section 2.3.

[20] The critical reflectance uncertainty due to AOD variation, which is shown as the red or blue dashed lines above and below the simulated critical reflectance, generally increases as a function of SSA, and is also typically larger for the fine aerosol model. However, because the sensitivity of the critical reflectance to SSA also increases as a function of SSA, the effect of the uncertainty due to varying AOD is lessened at higher SSA values. Also, in some cases AOD information from MODIS or other instruments is available to constrain this uncertainty. For example, the MODIS Deep Blue algorithm is one data set currently providing AOD over this region at visible wavelengths [*Hsu et al.*, 2004, 2006]. Last, at this particular geometry and wavelength, the critical reflectance values for the fine and coarse model are very similar at SSAs above 0.95, indicating insensitivity to assumptions of particle size when absorption is low. This is shown by the difference between the set of green arrows at high R_{crit} and SSA, and gray arrows at lower R_{crit} and SSA. The two aerosol models result in a retrieved SSA difference of only 0.01 when R_{crit} is 0.35 and SSA $\sim$ 0.97, as compared with an SSA difference of 0.03 when R_{crit} is 0.25 and SSA = 0.905 to 0.935.

2.3. Inversion

[21] We determine an error associated with the inversion of critical reflectance to SSA by considering the uncertainty in the simulated critical reflectance-SSA relationship due to AOD variability and the uncertainty in the MODIS critical reflectance due to data fitting. The intersection of the upper limit of the MODIS critical reflectance value with the lower limit of the LUT curve becomes the upper limit of the

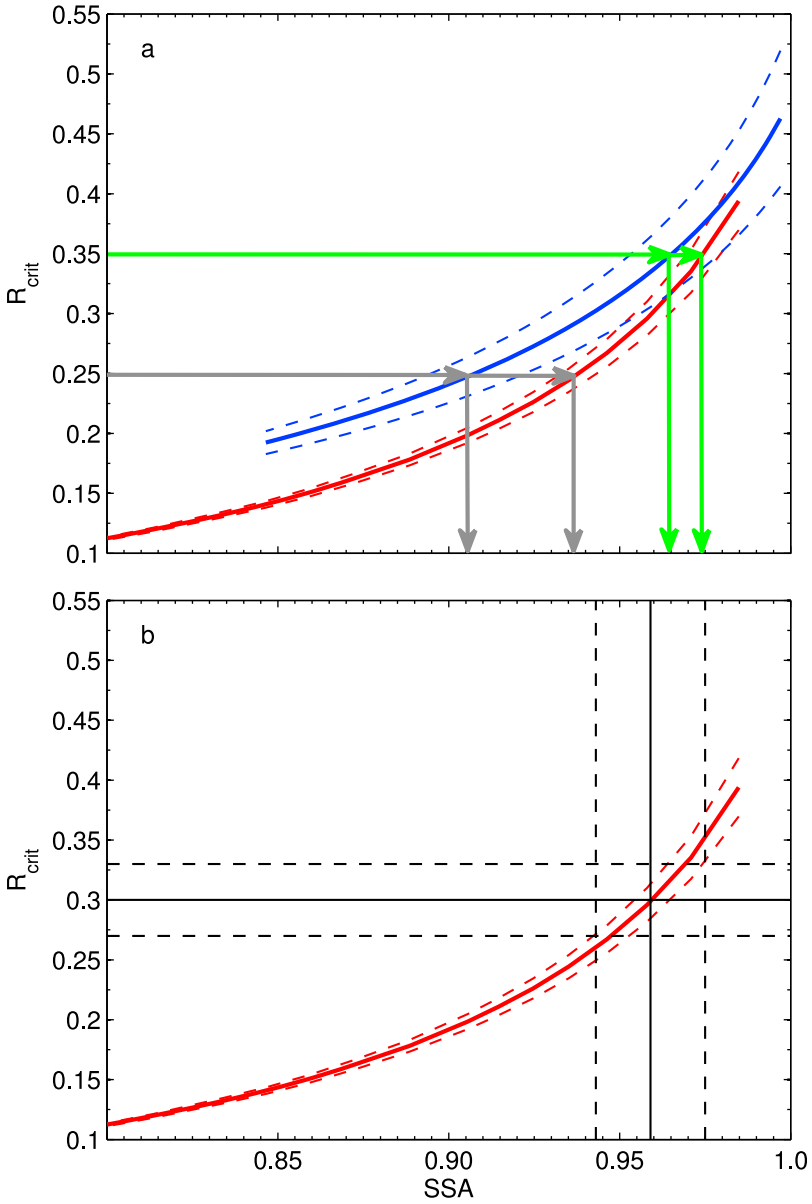

Figure 4. (a) R_{crit}-SSA curves for fine (blue) and coarse (red) aerosol models at 0.55 μm, SZA = 24°, view angle = 60°, and relative azimuth = 120°. Dashed lines represent the standard deviation of the intersections of the simulated TOA reflectance curves with the one-to-one line. Green lines indicate the inversion to SSA for R_{crit} = 0.35, and gray lines indicate the inversion to SSA for R_{crit} = 0.25. (b) Example determination of the inversion uncertainty of the retrieved SSA for the coarse model at 0.55 μm, SZA = 24°, view angle = 60°, and relative azimuth = 120° for a retrieved R_{crit} of 0.3 with an uncertainty of ±0.03.

retrieved SSA value; the intersection of the lower limit of the MODIS critical reflectance value with the upper limit of the LUT curve becomes the lower limit of the retrieved SSA. The example in Figure 4b demonstrates this for the coarse aerosol model example shown in Figure 4a. An observed critical reflectance of 0.3 with an uncertainty of ±0.03 corresponds to a retrieved SSA of 0.958 ± 0.015 at this particular wavelength, solar and viewing geometry. Again, note that this final SSA uncertainty only takes into account the uncertainty in the measurements and the uncertainty in the simulated R_{crit} due to AOD variability. It does not account for additional uncertainty due to model assumptions, which are discussed in section 2.4. An additional source of error not discussed here may result from the use of a scalar radiative transfer code (SBDART) to construct the LUT. This simplification of the radiative transfer calculation will primarily affect the SSA retrieved at 0.47 μm [*Levy et al.*, 2004]. Although we believe the sensitivity of the critical reflectance to aerosol and Rayleigh scattering polarization will be small, future studies should attempt to quantify this uncertainty.

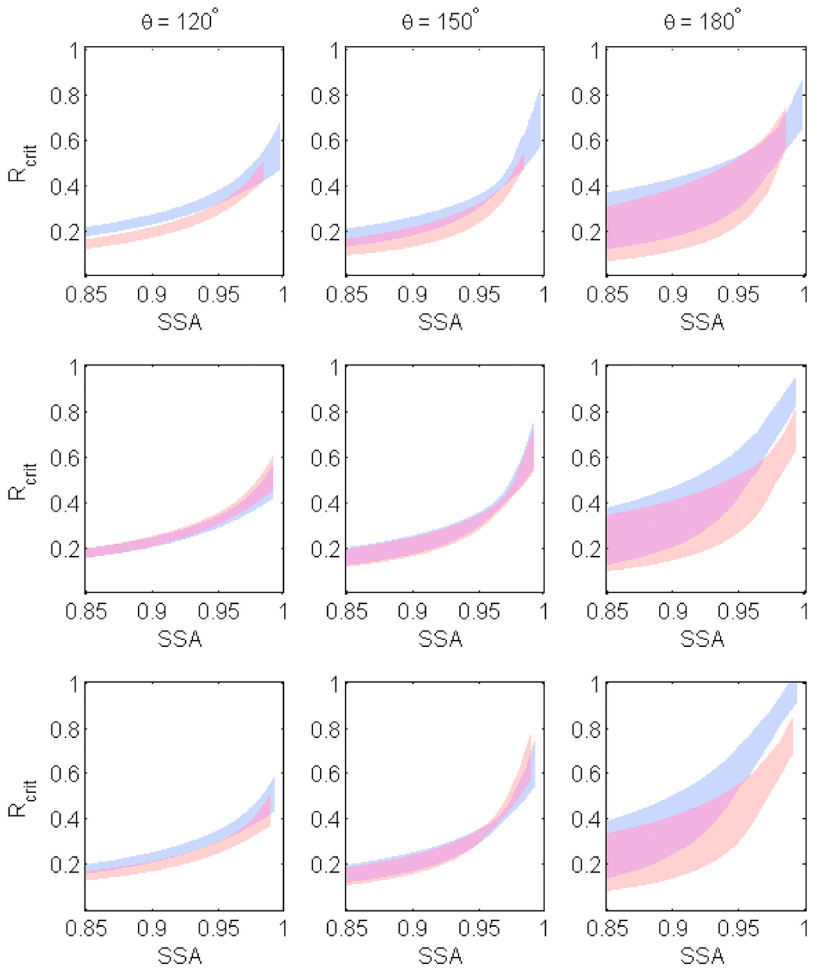

Figure 5. Average critical reflectance-SSA curves at 0.55 μm for scattering angles of (left) 120°, (middle) 150°, and (right) 180°. Shaded area represents the mean ± one standard deviation in critical reflectance for each SSA and scattering angle; it does not represent a retrieval uncertainty. Top plots correspond to the fine aerosol model (blue) and the coarse aerosol model (red), middle plots correspond to the bimodal sphere model (blue) and spheroid model (red), and bottom plots correspond to the bimodal sphere model for n_r = 1.63 (blue) and for n_r = 1.43 (red).

2.4. Sensitivity of Critical Reflectance to Aerosol Size, Shape, and Refractive Index

[22] Example R_{crit}-SSA LUT results for the fine and coarse aerosol models at 0.55 μm and for the bimodal spheres and spheroid models are shown in the top and middle plots of Figure 5, respectively. Because a large range of solar and viewing geometries were simulated, we group the results by scattering angle to present them here. In doing so, some of the sensitivities exposed by looking at a particular geometry (Figure 4a) are lost. Still, the scattering angle simplification reveals important generalities. All results within ±1° of scattering angle = 120°, 150°, and 180° are compiled; the shaded areas correspond to the average R_{crit}-SSA relationship bounded by one standard deviation on either side of the mean. As such, the spread does not represent a retrieval uncertainty, but simply the variety of geometries that can represent a specific scattering angle for the MODIS platform. These curves could not be inverted to perform a retrieval of SSA.

[23] At 0.55 μm the average results show several important sensitivities of the retrieval. First, the difference between choice of fine and coarse model (Figure 5, top) matters more than the difference between spherical and spheroid models (Figure 5, middle) throughout most of the geometry encountered, and particularly at smaller scattering angles. Second, it is only for scattering angles approaching 180° that the retrieval becomes very sensitive to the assumption of shape as spherical versus spheroid. The direct backscattering direction (180°) will introduce large uncertainties in the retrieval and should be avoided. This was noted by *Kaufman* [1987], who suggested that scattering angles between 120° and 160° were optimal for the success of the critical reflectance method. Third, the less absorbing the aerosol, the greater the sensitivity to particle shape, while the more absorbing the aerosol, the greater the sensitivity to particle size.

[24] To test the sensitivity of the critical reflectance to the assumed real part of the refractive index (n_r) of the aerosol, we perform two test simulations in SBDART for the

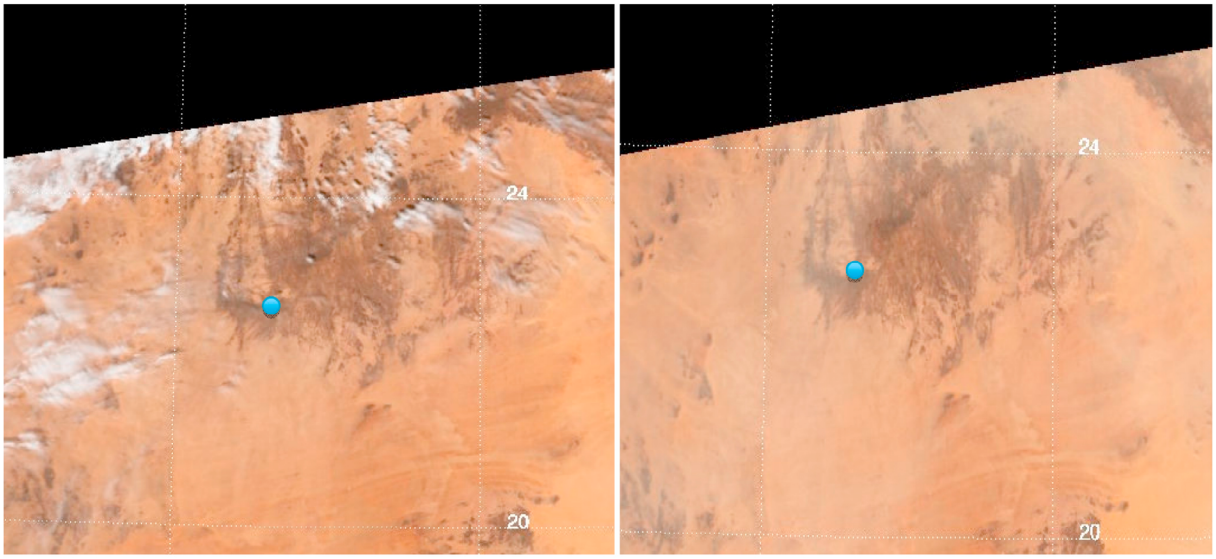

Figure 6. MODIS RGB images for (left) 6 February 2007, the cleaner day, and (right) 22 February 2007, the polluted day. The blue dot indicates the location of the Tamanrasset AERONET site. Images are taken from the MODIS Atmospheres Web site (www.modis-atmos.gsfc.nasa.gov).

bimodal sphere model, one with n_r = 1.43, and another with n_r = 1.63. This range is probably more extreme than that found in nature, particularly at the values on the higher end, so this test represents the upper bound of uncertainty for the assumed refractive index. The results are shown in the bottom plots of Figure 5. As with the assumption of particle shape, the impact of the assumption of refractive index is generally low, although it can be significant at a scattering angle of 180° when aerosol absorption is low.

[25] To summarize, these results show that our ability to derive SSA from R_{crit} is insensitive to assumptions of the aerosol shape and real part of the refractive index, although as absorption decreases and as the scattering angle approaches 180° these assumptions become more important. Conversely, our results show that as absorption increases, the retrieval becomes more sensitive to the assumed particle size. On the basis of the results presented here, we hypothesize that our application of the critical reflectance retrieval over North Africa, where the dominant aerosol type is dust with mainly low-absorbing SSA > 0.95 over most of the spectral range, may be subject to larger uncertainties due to assumptions of shape, refractive index, and AOD variability than if we apply the method in a region impacted by more absorbing aerosol. However, the increased sensitivity of the critical reflectance to SSA at higher SSA may help to compensate for the contribution of model uncertainties in the final inversion to retrieve SSA.

3. Retrievals at Tamanrasset

[26] To test the critical reflectance method of deriving SSA over bright desert surfaces, we perform retrievals over two North African AERONET sites. The first is Tamanrasset INM, a site in the Algerian Sahara (N 22° 47′ 22″, E 05° 31′ 48″). In order to find cases with a 16 day separation that have different aerosol loadings, we utilize the Version 2 Level 2 AOD data from each site. Pairs of days are chosen so that the 0.44 μm AOD is less than 0.2 on the cleaner day, and greater than 0.4 on the polluted day. We choose a cutoff of $AOD_{0.44\mu m}$ = 0.4 to define the polluted day because the uncertainty in the AERONET inversions is reduced at AODs above this value [*Dubovik et al.*, 2000]. We choose a cutoff of $AOD_{0.44\mu m}$ = 0.2 for the cleaner day in order to ensure some separation in aerosol loading between the two days, but it should be noted that a near-zero AOD for the cleaner day is not a requirement for the critical reflectance method; it simply relies on an AOD difference between the two comparison days. Eighteen pairs of days are chosen at Tamanrasset from 2007 and 2008. Some days have both Terra and Aqua data available, and a few days had cleaner cases for +16 and −16 days from the polluted day available for comparison, making a total of 24 paired cases at Tamanrasset.

[27] Given its location, the Tamanrasset AERONET site should be impacted primarily by soil dust aerosol. The average 0.44–0.87 μm Angstrom exponent at this site is 0.16 for cases when the 0.44 μm AOD exceeds 0.4, indicating that aerosol events at this site are dominated by coarse particles. Figure 6 shows an Aqua MODIS RGB image of the Tamanrasset location and the surrounding region that will be used to retrieve the SSA of the dust. The dusty day is 22 February 2007 and the cleaner day is 6 February 2007. The overpass time is 1250 UTC. Because the solar and satellite geometry is the same, the satellite overpasses the location at the same time on both days.

[28] Applying the retrieval across the image as described above, using the coarse mode model, yields maps of the critical reflectance and SSA, shown in Figures 7a and 7b at 0.55 μm. Missing pixels are due to the screening of clouds, missing reflectances within the retrieval pixel, or too much scatter as determined by the robust fitting routine. It should be noted that the area north of 22°N between 5° and 7°E often yields poor fits to the reflectance data, despite the fact that many of the pixels are retained by the algorithm. The

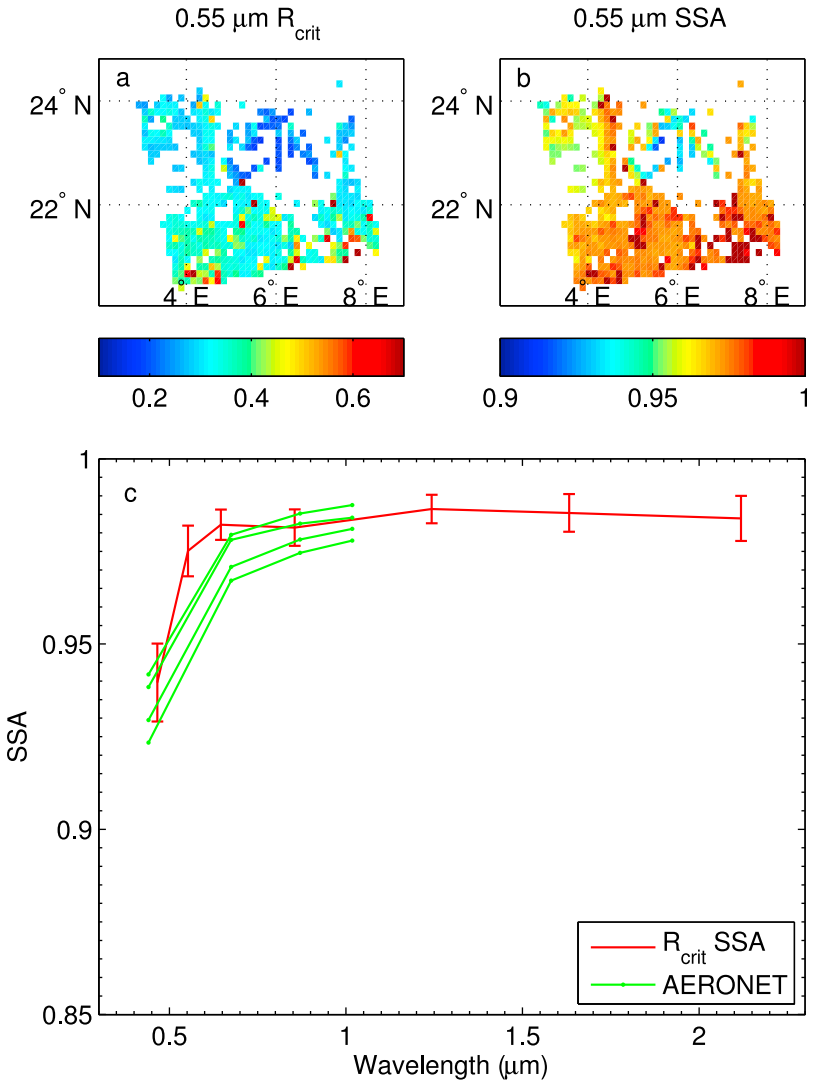

Figure 7. (a) 22 February 2007, 0.55 μm R_{crit}, (b) 0.55 μm SSA, and (c) spectral SSA at Tamanrasset from MODIS (R_{crit} SSA, red) and AERONET (green).

critical reflectances retrieved here are generally much lower than over the rest of the image, and are not representative of the actual critical reflectance based on a visual inspection of the scatterplots. Thus, we focus our attention on the portions of the image that are south and west of this area.

[29] As shown in Figure 7a, results for 22 February 2007 give critical reflectance values at 0.55 μm between 0.3 and 0.4, with some intermittent pixels exceeding 0.5 and 0.6. The 0.55 μm SSA values (Figure 7b) for this case fall mostly in the range between 0.97 and 0.98, although values are a bit lower near the cloudy area, which could be due to incomplete removal of cloudy pixels. A few have been set to a value of 1.0; any pixel in which the critical reflectance exceeds the maximum value in the LUT is set to 1.0. The critical reflectance of these pixels is generally higher than the surrounding pixels, which could indicate that the background aerosol is varying across the image. The few pixels that remain in the area north of 22°N between 5° and 7°E have SSA values that appear much more absorbing than the rest of the pixels in the image, again owing to a poor determination of the critical reflectance. One reason for this poor determination may be the existence of complex topography in the region, as Tamanrasset is located near the Ahaggar Mountains in southern Algeria. Complex topography can complicate the critical reflectance retrieval; there is increased sensitivity to small misalignments in solar and viewing geometry between the polluted and cleaner days because of the 3-D aspect of the terrain. An additional complication is the increased spatial heterogeneity in AOD due to the heterogeneity in surface elevation.

[30] In order to investigate the spectral behavior of the SSA, and to facilitate comparisons with data from the Tamanrasset AERONET station, we calculate 5 × 5 pixel (~75 × 75 km) averages of the critical reflectance and SSA near the Tamanrasset site. Because the site itself is located in the region where good retrievals could rarely be performed, all comparisons are to MODIS data located 1° latitude south of the station, where much better data regressions could be achieved and spatial variability of the results is much lower. The spectral results of the SSA retrieval for the 22 February 2007 case for all seven MODIS wavelengths retrieved are shown in Figure 7c, with error bars that represent the average

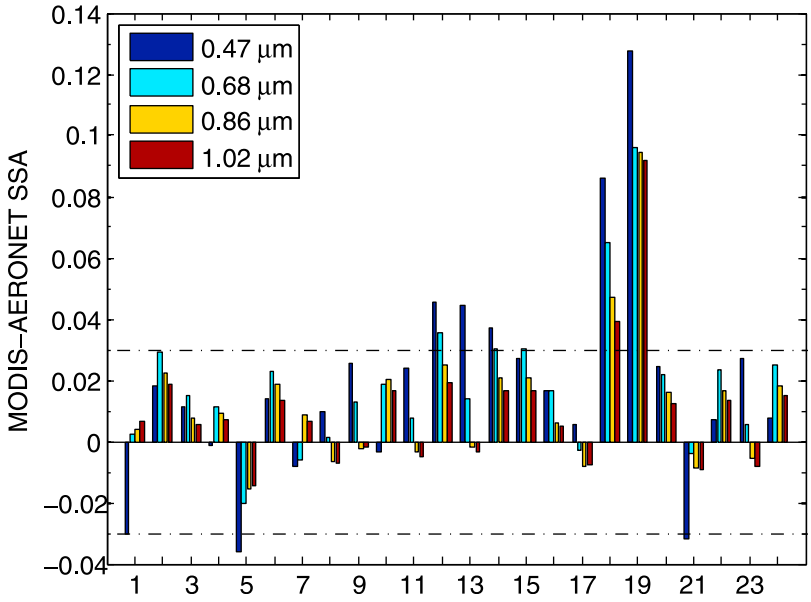

Figure 8. Spectral MODIS-AERONET differences in SSA for the retrieval cases at Tamanrasset. Wavelengths are interpolated to match two MODIS (0.47 and 0.86 μm) and two AERONET (0.68 and 1.02 μm) channels.

of the fitting uncertainties of each of the pixels that went into calculating the mean (σ_{mean}). The uncertainty estimate is calculated as

$$\sigma_{mean} = \sqrt{\frac{\sum_{i=1}^{N} \sigma_{SSA,i}^2}{N^2}}, \quad (2)$$

where $\sigma_{SSA,i}$ is the fitting uncertainty of each individual pixel and N is the number of pixels that went into the calculation of the spatial average (25 if there were no missing data in the vicinity). Also shown in Figure 7c are the Version 2 Level 1.5 AERONET SSA values determined from the AERONET sky radiances on that day. There are four reported AERONET retrievals at Tamanrasset on 22 February 2007, and none are identically coincident in time with the Aqua MODIS overpass. Note that AERONET retrieves at only four wavelengths, 0.44, 0.68, 0.87 and 1.02 μm at Tamanrasset.

[31] To examine quantitatively how the spectral dependence of the MODIS results compares to the AERONET spectral dependence, we interpolate the results spectrally to achieve SSA at four wavelengths, two of which correspond to AERONET channels (0.68 and 1.02 μm) and two of which correspond to MODIS channels (0.47 and 0.86 μm). The difference between the interpolated MODIS and AERONET values for each case are shown in Figure 8, with dashed lines representing the reported AERONET uncertainty of $\pm$0.03 [*Dubovik et al.*, 2000]. At Tamanrasset, differences between the two data sets are often largest at 0.47 μm, although seven of the cases exhibit the largest differences at 0.68 μm. The MODIS R_{crit} SSAs are usually less absorbing than the AERONET values and tend to exhibit similar spectral dependence. SSA differences decrease slightly with wavelength, but nearly all values in the near-IR are within the AERONET uncertainty bounds.

[32] The average MODIS-derived and AERONET-retrieved SSA values for the 27 cases at Tamanrasset are shown in Figure 9. The average results for MODIS have the same spectral signature and fall within one standard deviation of the AERONET values, although the MODIS average values are overall less absorbing than the AERONET results by approximately 0.01. A measure of average Saharan dust SSA, also using critical reflectance applied to MODIS data, is given by *Yoshida and Murakami* [2008], who also use a critical reflectance method applied to MODIS observations. The MODIS-derived mean SSA at Tamanrasset agrees to within 0.005 with *Yoshida and Murakami*'s [2008] values at 0.47 μm and 0.55 μm of 0.936 and 0.976, respectively. We have also included the average of MODIS Deep Blue SSA retrievals for the Tamanrasset cases (Deep Blue are not yet available from Terra for 2008, so this average is for a subset of the retrieval cases—Terra and Aqua for 2007, and Aqua for 2008). Note that the Deep Blue retrieval holds the SSA fixed at 0.65 μm, and retrieves the SSA at 0.41 and 0.47 μm. Deep Blue also indicates a less absorbing aerosol than AERONET, and agrees with the MODIS critical reflectance estimate at 0.47 μm within 0.01. Figures 7–9 demonstrate how the critical reflectance method can match the spectral dependence and magnitude of the ground-based and other satellite retrievals in dusty conditions. However, the importance of Figures 7–9 is to show how the critical reflectance method can expand aerosol absorption characterization spatially, across an image, and across the spectral range used for aerosol monitoring.

4. Retrievals at Banizoumbou

[33] The AERONET station at Banizoumbou (N 13° 32′ 27″, E 02° 39′ 54″) presents another opportunity to test the critical reflectance method over desert in a somewhat different aerosol situation. At Tamanrasset we could be confident that all aerosol events would be desert dust that could be represented with the coarse model. In contrast, the aerosol at Banizoumbou is often a mixture of dust transported from the

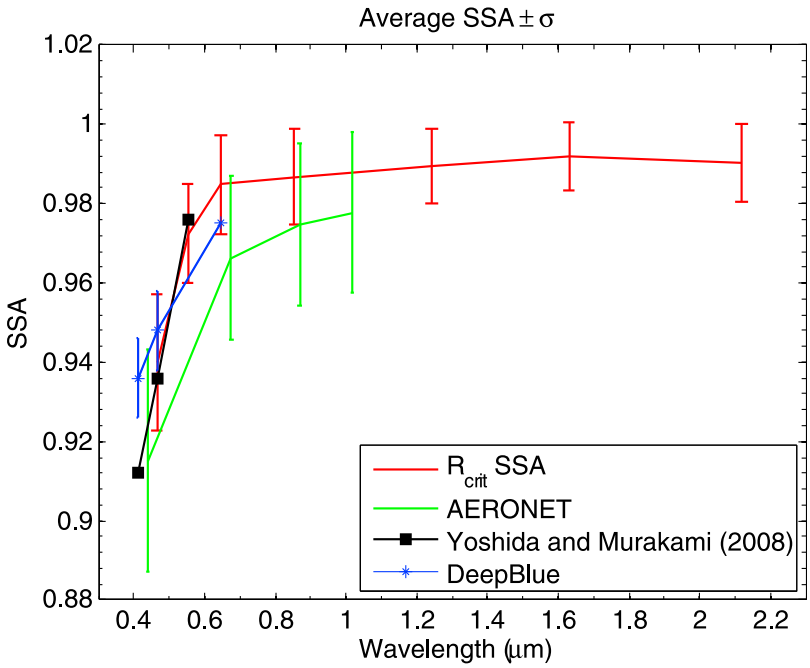

Figure 9. Average spectral SSA for the retrieval cases at Tamanrasset from MODIS critical reflectance (R_{crit} SSA, red), AERONET (green), *Yoshida and Murakami* [2008] (black), and MODIS Deep Blue (blue).

north and locally produced smoke or organic pollution [e.g., *Haywood et al.*, 2008]. Given this prevalence of more absorbing aerosol species, choosing a representative aerosol model (coarse, fine or bimodal) becomes more important in the retrieval. Additionally, the assumption of aerosol phase function and SSA being similar between the two days is more likely to be violated, which adds an additional source of uncertainty at this site. *Zhu et al.* [2011] tested the sensitivity of the retrieved SSA in biomass burning regimes to varying SSA on the cleaner day and found an uncertainty of up to 0.026 at 0.68 μm for a polluted day with SSA of $\sim$0.9. As such, we expect our uncertainty at this site will likely be

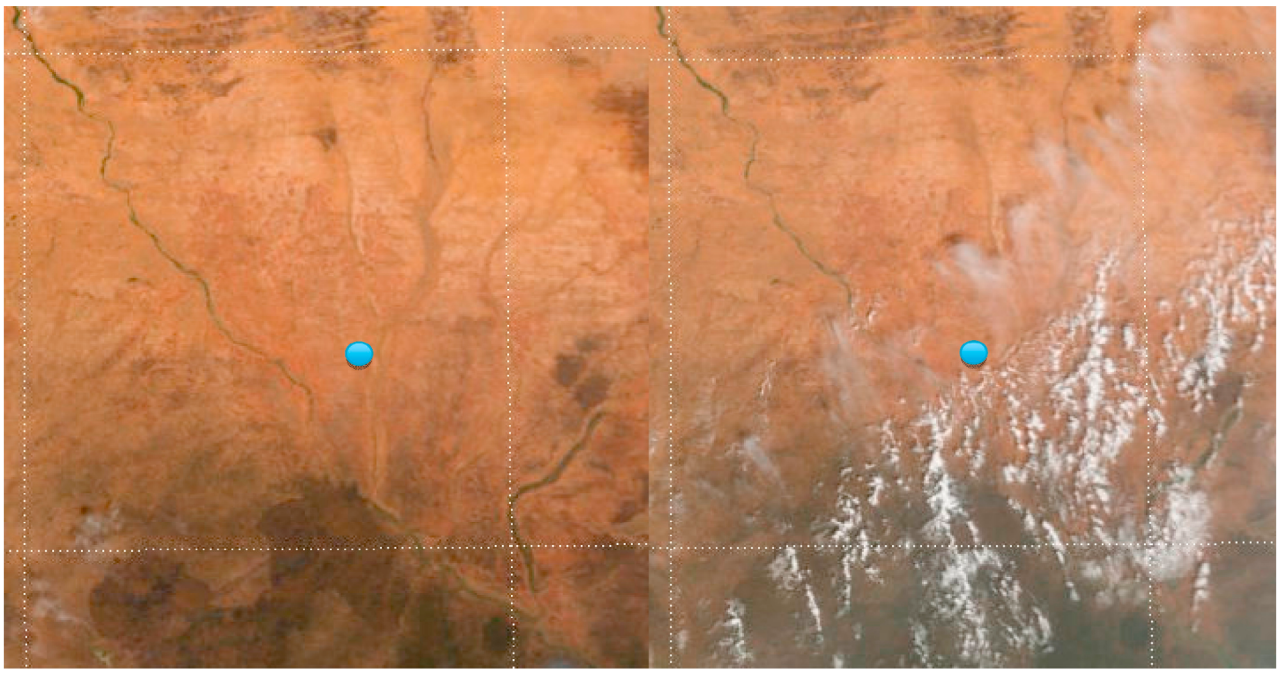

Figure 10. MODIS RGB images for (left) 26 November 2006, the cleaner day, and (right) 10 November 2006, the polluted day. The blue dot indicates the location of the Banizoumbou AERONET site. Images are taken from the MODIS Atmospheres Web site (www.modis-atmos.gsfc.nasa.gov).

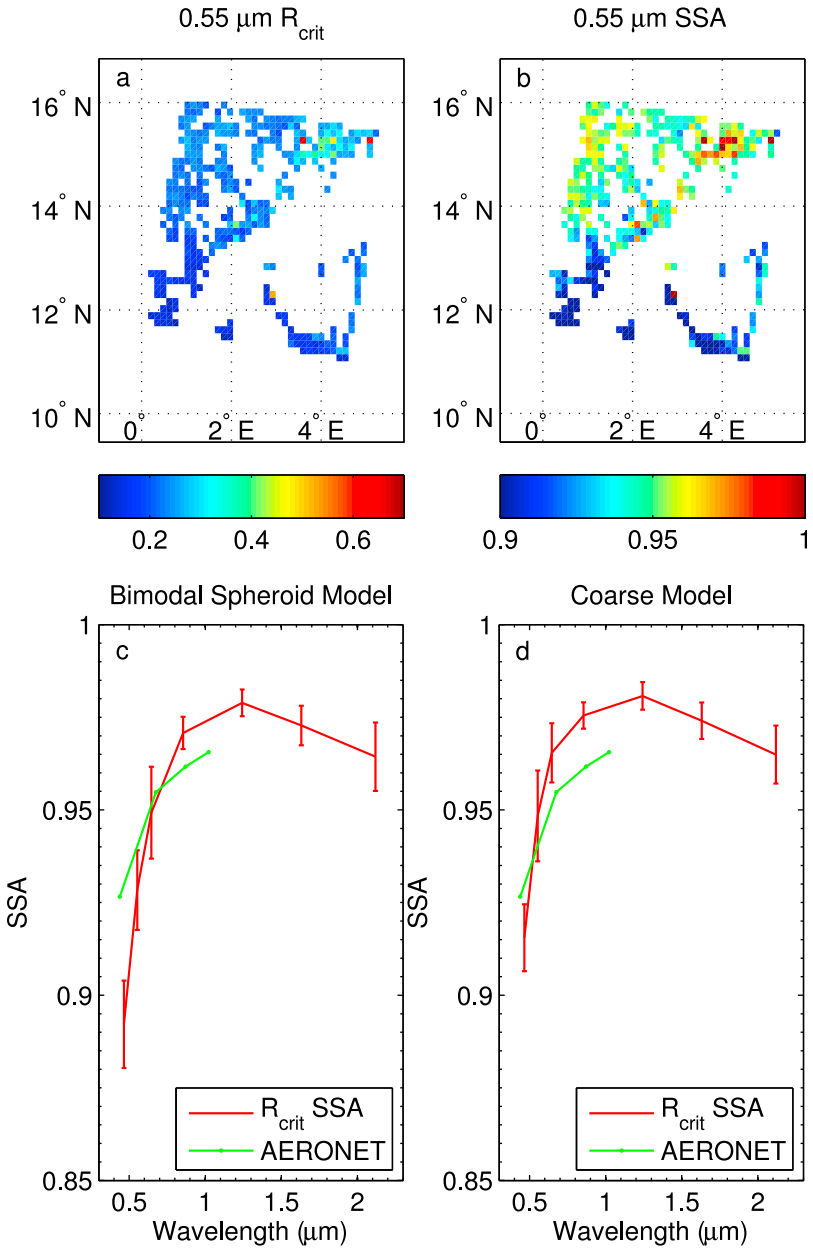

Figure 11. (a) 26 November 2006, 0.55 μm R_{crit}, (b) 0.55 μm SSA calculated using the coarse aerosol model, (c) spectral SSA at Banizoumbou from MODIS (R_{crit} SSA, red) for the bimodal spheroid model, and (d) spectral SSA at Banizoumbou for the coarse model. The AERONET retrieval closest to the MODIS overpass time is also shown (green).

similar to or greater than the uncertainty associated with the AERONET retrieval. We use the same 0.44 μm AOD criteria to find 15 cases at Banizoumbou, and apply the critical reflectance to each of the cases twice, once with the bimodal spheroid model and once with the coarse model.

[34] Figure 10 contains a Terra MODIS RGB image of the location of the Banizoumbou AERONET station and the surrounding area. The cleaner day is 26 November 2006, the polluted day is 10 November 2006, and the overpass time is 1035 UTC. Corresponding R_{crit} and SSA maps (retrieved for the coarse model) at 0.55 um are shown in Figures 11a and 11b, respectively. A significant portion of the image has been screened for clouds on this day; however, it is apparent that the R_{crit} values here are lower (0.2 to 0.3) than those observed at Tamanrasset and the corresponding SSA for the coarse model is lower ($\sim$0.95). Spectral SSA results using both the bimodal spheroid and coarse models with AERONET for comparison are shown in Figures 11c and 11d. The bimodal spheroid model yields more absorbing SSA values in the visible than the coarse model, but both models yield similar results in the near-IR channels.

[35] The spectral MODIS-AERONET differences by case are shown in Figure 12a for the bimodal spheroid model and

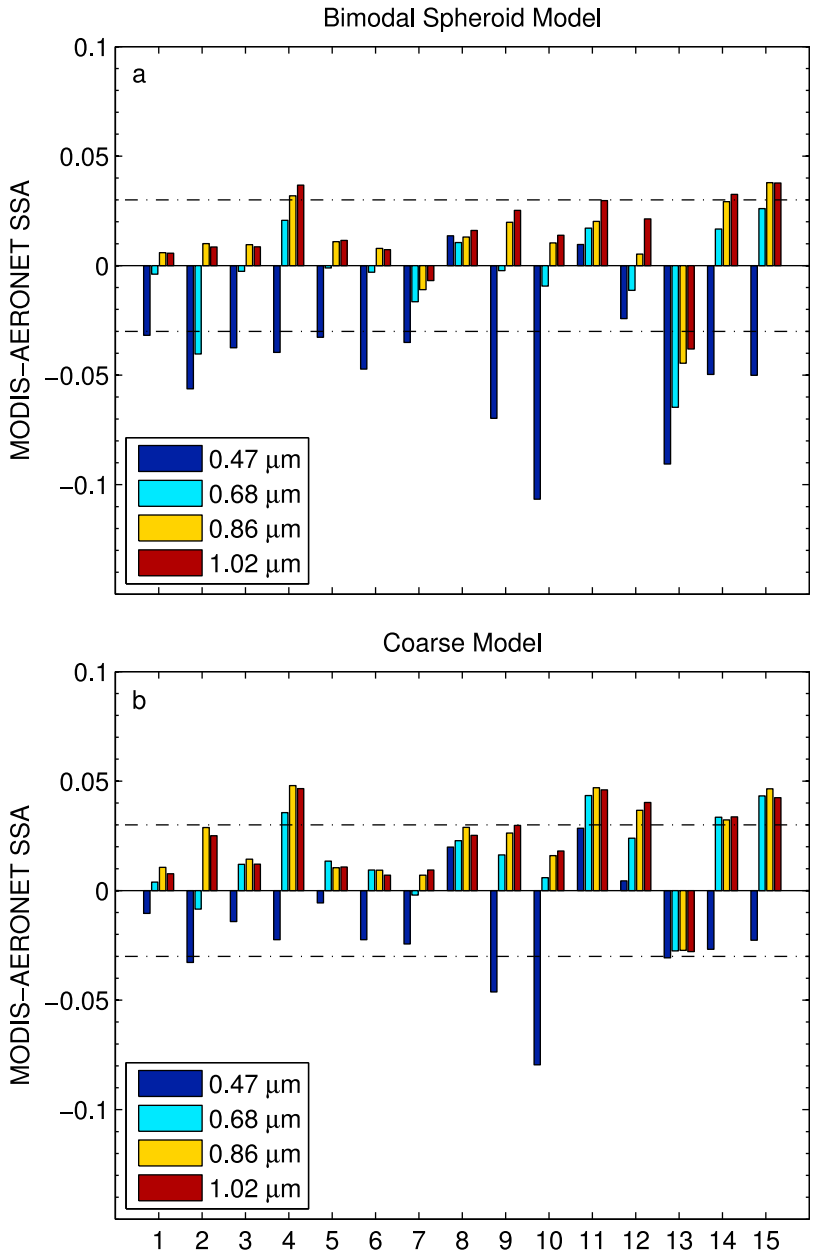

Figure 12. (a) Spectral MODIS-AERONET differences in SSA for the retrieval cases at Banizoumbou for the bimodal spheroid model and (b) spectral SSA differences for the coarse model. Wavelengths are interpolated to match two MODIS (0.47 and 0.86 μm) and two AERONET (0.68 and 1.02 μm) channels.

Figure 12b for the coarse model. MODIS SSA is generally brighter than AERONET in the near-IR, and more absorbing than AERONET at 0.47 μm. For the bimodal spheroid model differences are largest at 0.47 μm, followed by 1.02 μm, with the smallest differences occurring at 0.68 μm. The coarse model yields better agreement at 0.47 μm, but worse agreement in the longer-wavelength channels, as most of the cases are within the AERONET uncertainty bounds in the near-IR channels for the bimodal spheroid model.

[36] The average spectral results compared with AERONET retrievals are shown in Figure 13. Both models produce MODIS retrievals that match the average AERONET results to within the standard deviation of the AERONET retrieval in the midvisible range. The bimodal model (Figure 13a) produces a SSA value at 0.47 μm that is 0.04 lower than AERONET, but still within one standard deviation of the AERONET values. The coarse mode model better matches at 0.47 μm, but underestimates SSA relative to AERONET at 0.86 and 1.02 μm by 0.02. The average 0.47 μm Deep Blue SSA value at this site is the same as at Tamanrasset (0.948), although the variability is greater. This value only exceeds the AERONET results by about 0.02. At longer wavelengths than 1.02 μm, the MODIS retrieval produces an interesting spectral dependence for SSA, peaking at 1.24 μm. There is no way to

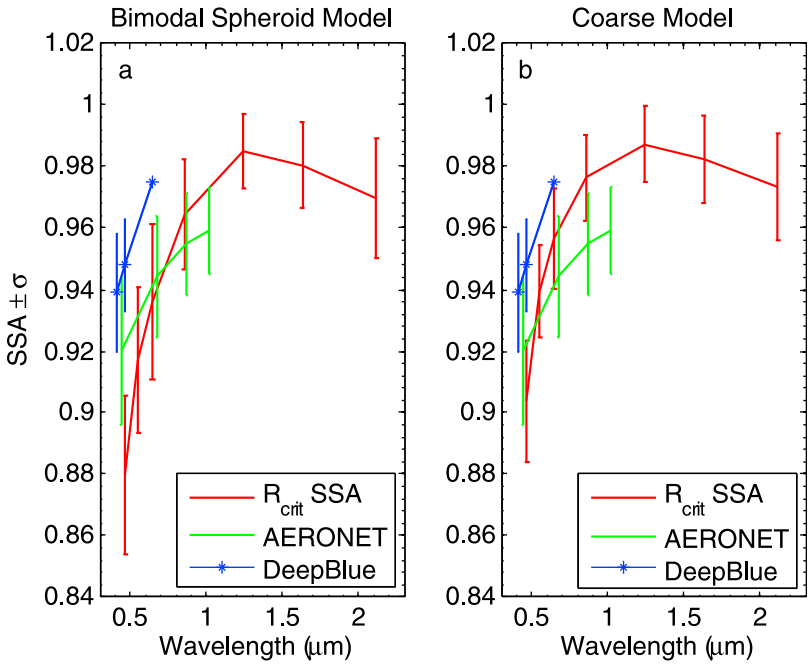

Figure 13. Average spectral SSA for the retrieval cases at Banizoumbou from MODIS critical reflectance (R_{crit} SSA, red), AERONET (green), and MODIS Deep Blue (blue) for (a) the bimodal spheroid model and (b) the coarse model.

evaluate this spectral behavior because there are no total column measurements of aerosol absorption in this spectral range.

5. Summary and Conclusions

[37] The critical reflectance method to obtain spectral single scattering albedo from MODIS radiances offers a unique view of an important aerosol property that is difficult to obtain from space-based observations. The spectral dependence of the SSA in the spectral range from 0.47 to 2.13 μm, and the spatial distribution of SSA across an image are important yet rarely seen properties that the critical reflectance can provide over desert. The method yields retrievals of SSA of pure desert dust that match AERONET retrievals to generally within 0.02 on a day to day basis, and to within 0.01 in terms of representing the mean characteristics of the aerosol absorption properties over a two year period. In a situation with dust/smoke mixtures such as at Banizoumbou, the match to AERONET is generally within 0.03, although the spectral dependence does not match as well as at the site with pure dust.

[38] The MODIS retrievals of Saharan dust yield average values of SSA of 0.94 ± 0.02, 0.97 ± 0.01, 0.98 ± 0.01, 0.99 ± 0.01, 0.99 ± 0.01, 0.99 ± 0.01, and 0.99 ± 0.01 at wavelengths of 0.47 μm, 0.55 μm, 0.65 μm, 0.86 μm, 1.24 μm, 1.61 μm, and 2.13 μm, respectively. In the Sahel region with dust/smoke mixtures MODIS retrieves a darker, more absorbing aerosol with SSA values of 0.88 ± 0.03, 0.92 ± 0.02, 0.94 ± 0.03, 0.96 ± 0.02, 0.99 ± 0.01, 0.98 ± 0.01, 0.97 ± 0.02, for the same wavelengths assuming a bimodal spheroid aerosol model, and 0.90 ± 0.02, 0.94 ± 0.02, 0.96 ± 0.02, 0.98 ± 0.01, 0.99 ± 0.01, 0.98 ± 0.01, 0.97 ± 0.02 assuming a coarse aerosol model. At 0.47 μm, MODIS Deep Blue retrieves on average 0.95 ± 0.005 at Tamanrasset, and 0.95 ± 0.02 at Banizoumbou. These uncertainties correspond to 1σ in the variability of the retrieved values at each site.

[39] The SBDART simulations indicate that the sensitivity of SSA to the critical reflectance is greater as SSA and aerosol size increase, and that retrievals of SSA will be more certain for large aerosol that have low absorption, which is consistent with the lower uncertainties that we find at dust-dominated Tamanrasset. The presence of particles with stronger absorption will result in a critical reflectance that is more sensitive to changes in particle size, contributing additional uncertainty into the retrieval of dust-smoke mixtures. This is consistent with the results at Banizoumbou. The SBDART simulations also suggest that the sensitivity to assumed real refractive index and shape is low, although could be significant at higher SSAs as the scattering angle approaches 180°. As such, scattering angles near 180° should be avoided when applying the critical reflectance method, particularly in the case of pure dust.

[40] The critical reflectance method provides an opportunity to quantify aerosol absorption characteristics over wide swaths and a broad spectral range. Keeping in mind the sensitivities identified here, we expect to retrieve spectral SSA to within ±0.02 for pure dust. Dust-smoke mixtures present additional challenges but can at the very least be marked as significantly different than pure dust, either by magnitude of the absorption or spectral signature. The impact of variable SSA between clean and polluted days, and the increased sensitivity to assumptions of particle size in these regimes add to the uncertainty in the critical reflectance determination. By applying the critical reflectance method to the almost 12 years of MODIS imagery over

the desert regions of the world, we anticipate a comprehensive characterization of the spectral absorption characteristics of desert dust and the narrowing of uncertainties in estimates of the radiative effect of dust over desert regions.

[41] **Acknowledgments.** This work was supported by the Center for Earth-Atmosphere Studies through NASA grant NNX08AT77G, with additional funding from NOAA grant NA17RJ1228. We thank Didier Tanré, Emilio Cuevas-Agullo, and Mohamed Mimouni for their efforts in establishing and maintaining the Banizoumbou and Tamanrasset AERONET sites, and we thank the MODIS team for their efforts in calibration and maintenance of the MODIS instrument and data. We would also like to thank Li Zhu, Tom Eck, Rob Levy, Shana Mattoo, and the anonymous reviewers for their helpful suggestions in developing and revising this work.

References

de Almeida Castanho, A. D., J. V. Martins, and P. Artaxo (2008), MODIS aerosol optical depth retrievals with high spatial resolution over an urban area using the critical reflectance, *J. Geophys. Res.*, *113*, D02201, doi:10.1029/2007JD008751.

Dubovik, O., and M. D. King (2000), A flexible inversion algorithm for retrieval of aerosol optical properties from Sun and sky radiance measurements, *J. Geophys. Res.*, *105*, 20,673–20,696, doi:10.1029/2000JD900282.

Dubovik, O., A. Smirnov, B. N. Holben, M. D. King, Y. J. Kaufman, T. F. Eck, and I. Slutsker (2000), Accuracy assessments of aerosol optical properties retrieved from Aerosol Robotic Network (AERONET) Sun and sky radiance measurements, *J. Geophys. Res.*, *105*, 9791–9806, doi:10.1029/2000JD900040.

Dubovik, O., B. N. Holben, T. Lapyonok, A. Sinyuk, M. I. Mishchenko, P. Yang, and I. Slutsker (2002), Non-spherical aerosol retrieval method employing light scattering by spheroids, *Geophys. Res. Lett.*, *29*(10), 1415, doi:10.1029/2001GL014506.

DuMouchel, W. H., and F. L. O'Brien (1989), Integrating a robust option into a multiple linear regression computing environment, paper presented at Computer Science and Statistics: The 21st Symposium on the Interface, Am. Stat. Assoc., Alexandria, Va.

Fraser, R. S., and Y. J. Kaufman (1985), The relative importance of aerosol scattering and absorption in remote-sensing, *IEEE Trans. Geosci. Remote Sens.*, *GE-23*, 625–633, doi:10.1109/TGRS.1985.289380.

Haywood, J. M., et al. (2008), Overview of the Dust and Biomass-burning Experiment and African Monsoon Multidisciplinary Analysis Special Observing Period-0, *J. Geophys. Res.*, *113*, D00C17, doi:10.1029/2008JD010077.

Herman, R. J., P. K. Bhartia, O. Torres, C. Hsu, C. Seftor, and E. Celarier (1997), Global distribution of UV-absorbing aerosols from Nimbus 7/TOMS data, *J. Geophys. Res.*, *102*, 16,911–16,922, doi:10.1029/96JD03680.

Holben, B. N., et al. (1998), AERONET: A federated instrument network and data archive for aerosol characterization, *Remote Sens. Environ.*, *66*, 1–16, doi:10.1016/S0034-4257(98)00031-5.

Hsu, N. C., J. R. Herman, P. K. Bhartia, C. J. Seftor, O. Torres, A. M. Thompson, J. F. Gleason, T. F. Eck, and B. N. Holben (1996), Detection of biomass burning smoke from TOMS measurements, *Geophys. Res. Lett.*, *23*, 745–748, doi:10.1029/96GL00455.

Hsu, N. C., S.-C. Tsay, M. D. King, and J. R. Herman (2004), Aerosol properties over bright-reflecting source regions, *IEEE Trans. Geosci. Remote Sens.*, *42*, 557–569, doi:10.1109/TGRS.2004.824067.

Hsu, N. C., S.-C. Tsay, M. D. King, and J. R. Herman (2006), Deep Blue retrievals of Asian aerosol properties during ACE-Asia, *IEEE Trans. Geosci. Remote Sens.*, *44*, 3180–3195, doi:10.1109/TGRS.2006.879540.

Jeong, M.-J., and N. C. Hsu (2008), Retrievals of aerosol single-scattering albedo and effective aerosol layer height for biomass burning smoke: Synergy derived from "A-train" sensors, *Geophys. Res. Lett.*, *35*, L24801, doi:10.1029/2008GL036279.

Johnson, B. T., B. Heese, S. A. McFarlane, P. Chazette, A. Jones, and N. Bellouin (2008), Vertical distribution and radiative effects of mineral dust and biomass burning aerosol over West Africa during DABEX, *J. Geophys. Res.*, *113*, D00C12, doi:10.1029/2008JD009848.

Johnson, B. T., S. Christopher, J. M. Haywood, S. R. Osborne, S. McFarlane, C. Hsu, C. Salustro, and R. Kahn (2009), Measurements of aerosol properties from aircraft, satellite and ground-based remote sensing: A case-study from the Dust and Biomass-burning Experiment (DABEX), *Q. J. R. Meteorol. Soc.*, *135*, 922–934, doi:10.1002/qj.420.

Kahn, R. A., B. J. Gaitley, M. J. Garay, D. J. Diner, T. F. Eck, A. Smirnov, and B. N. Holben (2010), Multiangle Imaging SpectroRadiometer global aerosol product assessment by comparison with the Aerosol Robotic Network, *J. Geophys. Res.*, *115*, D23209, doi:10.1029/2010JD014601.

Kalashnikova, O. V., and R. Kahn (2006), Ability of multiangle remote sensing observations to identify and distinguish mineral dust types: 2. Sensitivity over dark water, *J. Geophys. Res.*, *111*, D11207, doi:10.1029/2005JD006756.

Kaufman, Y. J. (1987), Satellite sensing of aerosol absorption, *J. Geophys. Res.*, *92*, 4307–4317, doi:10.1029/JD092iD04p04307.

Kaufman, Y. J., A. E. Wald, L. A. Remer, B. C. Gao, R. R. Li, and L. Flynn (1997), The MODIS 2.1-mu m channel: Correlation with visible reflectance for use in remote sensing of aerosol, *IEEE Trans. Geosci. Remote Sens.*, *35*, 1286–1298, doi:10.1109/36.628795.

Kaufman, Y. J., D. Tanré, O. Dubovik, A. Karnieli, and L. A. Remer (2001), Absorption of sunlight by dust as inferred from satellite and ground-based remote sensing, *Geophys. Res. Lett.*, *28*, 1479–1482, doi:10.1029/2000GL012647.

Levy, R. C., L. A. Remer, and Y. J. Kaufman (2004), Effects of neglecting polarization on the MODIS aerosol retrieval over land, *IEEE Trans. Geosci. Remote Sens.*, *42*, 2576–2583, doi:10.1109/TGRS.2004.837336.

Liao, H., and J. H. Seinfeld (1998), Radiative forcing by mineral dust aerosols: Sensitivity to key variables, *J. Geophys. Res.*, *103*, 31,637–31,645, doi:10.1029/1998JD200036.

Martins, J. V., D. Tanré, L. Remer, Y. Kaufman, S. Mattoo, and R. Levy (2002), MODIS cloud screening for remote sensing of aerosols over oceans using spatial variability, *Geophys. Res. Lett.*, *29*(12), 8009, doi:10.1029/2001GL013252.

Remer, L. A., et al. (2005), The MODIS aerosol algorithm, products, and validation, *J. Atmos. Sci.*, *62*, 947–973, doi:10.1175/JAS3385.1.

Remer, L., D. Tanré, R. Levy, Y. Kaufman, and S. Mattoo (2006), Algorithm for remote sensing of tropospheric aerosol from MODIS: Collection 5, report, NASA Goddard Space Flight Cent., Greenbelt, Md.

Ricchiazzi, P., S. R. Yang, C. Gautier, and D. Sowle (1998), SBDART: A research and teaching software tool for plane-parallel radiative transfer in the Earth's atmosphere, *Bull. Am. Meteorol. Soc.*, *79*, 2101–2114, doi:10.1175/1520-0477(1998)079<2101:SARATS>2.0.CO;2.

Satheesh, S. K., O. Torres, L. A. Remer, S. S. Babu, V. Vinoj, T. F. Eck, R. G. Kleidman, and B. N. Holben (2009), Improved assessment of aerosol absorption using OMI-MODIS joint retrieval, *J. Geophys. Res.*, *114*, D05209, doi:10.1029/2008JD011024.

Solmon, F., M. Mallet, N. Elguindi, F. Giorgi, A. Zakey, and A. Konare (2008), Dust aerosol impact on regional precipitation over western Africa, mechanisms and sensitivity to absorption properties, *Geophys. Res. Lett.*, *35*, L24705, doi:10.1029/2008GL035900.

Stamnes, K., S. C. Tsay, W. Wiscombe, and K. Jayaweera (1988), Numerically stable algorithm for discrete-ordinate-method radiative-transfer in multiple-scattering and emitting layered media, *Appl. Opt.*, *27*, 2502–2509, doi:10.1364/AO.27.002502.

Torres, O., A. Tanskanen, B. Veihelmann, C. Ahn, R. Braak, P. K. Bhartia, P. Veefkind, and P. Levelt (2007), Aerosol and surface UV products from Ozone Monitoring Instrument observations: An overview, *J. Geophys. Res.*, *112*, D24S47, doi:10.1029/2007JD008809.

Yoshida, M., and H. Murakami (2008), Dust absorption averaged over the Sahara inferred from moderate resolution imaging spectroradiometer, *Appl. Opt.*, *47*, 1995–2003, doi:10.1364/AO.47.001995.

Yu, H., et al. (2006), A review of measurement-based assessments of the aerosol direct radiative effect and forcing, *Atmos. Chem. Phys.*, *6*, 613–666, doi:10.5194/acp-6-613-2006.

Zhu, L., J. V. Martins, and L. A. Remer (2011), Biomass burning aerosol absorption measurements with MODIS using the critical reflectance method, *J. Geophys. Res.*, *116*, D07202, doi:10.1029/2010JD015187.

S. Kreidenweis, Department of Atmospheric Science, Colorado State University, Campus Delivery 1371, Fort Collins, CO 80523, USA. (sonia@atmos.colostate.edu)

J. V. Martins, Department of Physics, University of Maryland, Baltimore County, 1000 Hilltop Cir., Baltimore, MD 21250, USA. (martins@umbc.edu)

L. Remer, NASA Goddard Space Flight Center, Code 613.2, Greenbelt, MD 20771, USA. (Lorraine.a.remer@nasa.gov)

G. L. Stephens, Jet Propulsion Laboratory, M/S 183-505, 4800 Oak Grove Dr., Pasadena, CA 91109, USA. (stephens@atmos.colostate.edu)

K. C. Wells, Department of Soil, Water and Climate, University of Minnesota, Twin Cities, 439 Borlaug Hall, 1991 Upper Buford Cir., Saint Paul, MN 55108, USA. (kcw@umn.edu)